6G Indoor Network Enabled by Photonics- and Electronics-Based sub-THz Technology

Sang-Rok Moon [ID], *Member, IEEE*, Eon-Sang Kim [ID], Minkyu Sung [ID], Hae Young Rha, Eui Su Lee [ID], IL-Min Lee, Kyung Hyun Park [ID], Joon Ki Lee, and Seung-Hyun Cho

Abstract—We propose an indoor network with a sub-terahertz-band wireless link for 6G applications. In our proposed indoor network, an optical hub unit (OHU) that controls the entire system is optically linked to THz remote nodes (RNs) over optical distribution fibers. The THz RNs communicate with the user equipment through a sub-THz wireless link. The function of the THz RNs is to provide an interface between the optical link and the sub-THz wireless link. For downlink transmission, a photonics-based sub-THz-band signal generation method is adopted to take advantage of the broadband characteristics of the optical components. An electronics-based sub-THz mixer is also used for uplink transmission because of its cost-effectiveness and low energy consumption. A digital signal processor (DSP) is designed to recover the original transmitted baseband signal. The DSP provides frequency offset compensation over a wide frequency range and reduces the probability of cyclic slip. The performance of the proposed system was investigated experimentally with commercially available optical/electrical components. We demonstrate 100 Gb/s 2.5-m wireless transmission with a 16-quadrature amplitude modulation (16-QAM) signal for configuring the downlink. The optical transmission distance was set to 10 km, and the power penalty measured by optical transmission was negligible. We also investigated the scalability and tunability of the photonics-based sub-THz transmitter to confirm the upgradability of our proposed indoor network to consider future capacity expansion. To establish an uplink, a 25 Gb/s 1.5-m wireless transmission with a quadrature phase shift keying (QPSK) signal was employed. A directly modulated laser was used for cost-effective optical transmission. Unlike downstream transmission, a measured bit error rate (BER) penalty caused by the optical transmission was observed. This is due to the interplay between the frequency chirp of the directly modulated laser and the chromatic dispersion in the fiber. Despite this penalty, BERs less than the soft-decision forward error correction (FEC) threshold (2×10^{-2}) with 20% overhead were achieved. We discuss several remaining technical challenges in real-field deployment. These include THz Tx power improvement, photonic integration, reducing form-factor, polarization insensitivity, and automatic beam steering. Our recent efforts to address these issues are also introduced and examined.

Index Terms—6G indoor network, high-speed transmission, sub-THz communication, sub-THz link, THz indoor network.

I. INTRODUCTION

RECENTLY, a few key innovations that are likely to impact our lives in a major way have been proposed. Examples include remote medical services, digital twins, virtual reality, and cooperative intelligent networks [1], [2]. One of the key enablers to bring them into reality is ultra-high-speed communication technology. The required data rate for these services is predicted to be greater than 100 Gb/s [3], [4]. To meet this requirement, the peak data rate of 6G communication systems, which are being actively discussed, is proposed to be in the range of 100 Gb/s–1 Tb/s [3]. To realize these data rates, an increase in carrier frequency is inevitable; thus, the sub-THz-band (0.2–3 THz) frequency has been suggested as a promising candidate. In particular, the 200–300 GHz frequency band has drawn considerable interest because of its accessibility for the implementation of an amplifier and a relatively low attenuation coefficient in the atmosphere. In the 200–300 GHz frequency band, several transmission results with a data rate of ∼100 Gb/s have already been shown using diverse technologies. The sub-THz-band signal can be generated using electronics- and photonics-based approaches. In electronics-based approaches, ∼100 Gb/s quadrature amplitude modulation (QAM)-based signal transmission has been demonstrated using high-speed integrated circuit (IC) technologies such as bipolar complementary metal–oxide–semiconductor (BiCMOS) [5], high-electron-mobility transistors (HEMTs) [6], and monolithic microwave integrated circuits (MMICs) [7]. In most photonics-based approaches, the sub-THz-band signal is generated by a uni-traveling-carrier photodiode (UTC-PD) that functions as a photomixer. With a UTC-PD, ∼100 Gb/s transmission has been demonstrated with QAM [8], orthogonal frequency division multiplexing (OFDM) [9], and pulse-amplitude modulation (PAM) [10] signal formats. Advanced digital signal processing (DSP) technologies, such as Kramers-Kronig receiver and probabilistic shaping, can be applied to improve the overall system performance [9], [11].

Sub-THz-band communication technology has high potential for various applications, such as wireless backhaul networks, in-factory reconfigurable communication, data showering, and chip-to-chip communication. Among them, an indoor network is considered to be a favorable application in the early development stage of sub-THz communication technology [12]. Because the sub-THz-band signal has a high directivity and a large free-space path loss (FSPL), it is suitable for an indoor network that has a short-range link with low moving speed.

To realize a THz indoor network in the near future, it is worth designing a network architecture and investigating its performance and the hurdles to be overcome. In this paper, we propose an indoor network with sub-THz-band communication technology. It is based on the conventional architecture of distributed antenna system (DAS) with radio-over-fiber technology (RoF) which have been widely investigated for 5G network [13]–[15]. In this architecture, fiber-optic link is used to connect central optical hub and remote antenna unit. Thanks to the high transmission capacity of fiber-optic link, this architecture is suitable to distribute high-speed data traffic into multiple nodes. By adopting this similar physical architecture with the RoF-DAS, cost-efficient and seamless upgrade will be possible in the near future. Both single-carrier and multi-carrier might be applied for sub-THz-band transmission [8], [9]. Multi-carrier modulation, such as OFDM, is robust to frequency-selective fading in a multipath environment. However, the sub-THz-band link in the indoor network might be assumed as a line-of-sight channel. Thus, single-carrier modulation was chosen for the sake of simple and fast realization.

In Section II, we describe the schematics of our proposed indoor network and explain its operating principles. For downstream transmission, we adopt photonics-based technology to take advantage of mature optical components in high-speed transmission. For generation of sub-THz signal, we employ an optical heterodyne mixing method with two free-running lasers. These lasers are separately placed at central optical hub unit and THz remote node. Comparing to the structure that phase-locked optical sources (e.g., optical comb) are placed at the OHU, this configuration is more tolerant of the optical link loss, which will be discussed later in detail. However, since the two lasers are not phase-locked, the frequency drift of the lasers and optical phase noise can generate frequency offset and cyclic slip, respectively. Thus, we carefully design a DSP which supports wide frequency offset compensation range using Chinese remainder theorem [16]. It also provides the probability of cyclic slip by using two-step carrier phase estimation. For the upstream link, the required data rate is expected to be lower than that of the downstream link. Thus, the upstream sub-THz-band signal is generated by electronics-based technology, considering the low power consumption and relatively simple structure of electronics-based technology. In Sections III and IV, we experimentally evaluate the performance of the proposed system. The experimental setup was established using commercially available optical/electrical components. In Section III, we demonstrate 100 Gb/s downstream transmission. This data rate is meaningful because it can be a milestone for the

key performance indicator (KPI) of 6G [4]. We also investigated the scalability of a photonics-based THz transmitter (Tx). The number of accommodatable THz remote nodes (RNs) can be expanded by employing power splitters. The power splitter induces optical link loss, so its effect on the system is measured and analyzed. To satisfy the 6G requirement of a 1 Tb/s peak data rate [3], the data throughput should be increased in the near future. One of the enabling technologies is frequency division multiplexing (FDM). To accomplish this, operation in a wide frequency band is mandatory. We investigated the tunability of the THz Tx and measured bit error rates (BERs) over a wide frequency range. Throughout the experiment, we confirmed the availability of data transmission inside the entire WR 3.4 band (220–330 GHz). In Section IV, we verify the performance of uplink transmission. We target the 25 Gb/s-class data rate, which is a quarter of the downlink speed. It is worth noting that we previously reported experimental investigations of upstream transmission performances [17]. Therefore, we focus only on the key results. In Section IV, we address several technical issues that need to be overcome for real-field deployment. Limited THz Tx power, bulkiness of optical components, form factors of the antenna, polarization dependency, and automatic beam steering are discussed. We then introduce a few promising technologies to solve these issues. Among them, we present some experimental results with UTC-PD employing a lens collimator that was developed by us, which has a smaller size compared with a UTC-PD with a horn antenna. Finally, we summarize our study in Section V.

II. PROPOSED THz INDOOR NETWORK

Fig. 1 shows a schematic diagram of the proposed THz indoor network. An optical hub unit (OHU), which is connected to the exterior network, is placed to provide centralized signal management for the THz indoor network. Each line card in the OHU includes a digital signal processor and an optical transceiver (TRx) and is connected to THz remote nodes (RNs) via distribution fibers. The THz RNs provide an interface between the fiber-optic link and the wireless link. The THz RNs communicate with the user equipment through a wireless channel. At the THz TRx and DSP chip in the user equipment, the sub-THz-band signal is up/down-converted from/to the baseband.

The detailed link structure is shown in Fig. 2(a). For downstream transmission, the Tx DSP in the line card generates a baseband QAM signal. Modulated optical light is then generated using an optical in-phase quadrature (IQ) modulator and laser diode (LD). The optical signal is amplified by an optical amplifier and then transmitted to the THz RN through an optical fiber. Two circulators were inserted to couple downstream and upstream transmission signal. The transmitted optical signal is combined with the output of the tunable laser, whose wavelength is separated by the corresponding sub-THz-band frequency. Before combining, their polarizations are aligned using a polarization controller. The combined light is amplified again and then injected into the UTC-PD after another
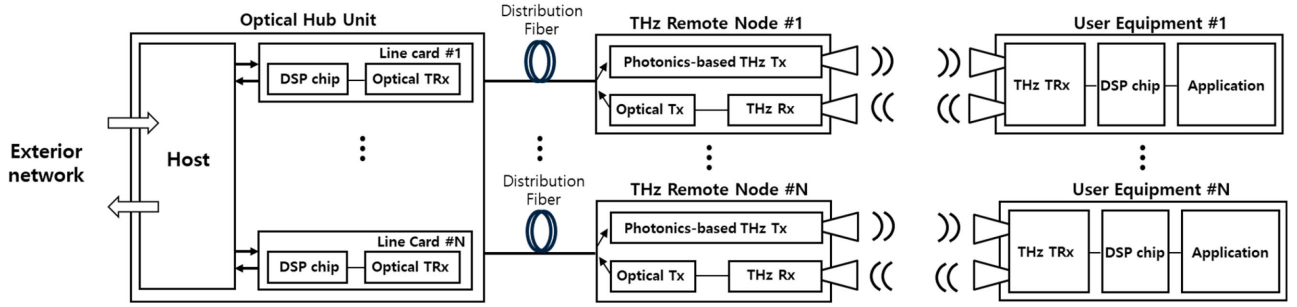
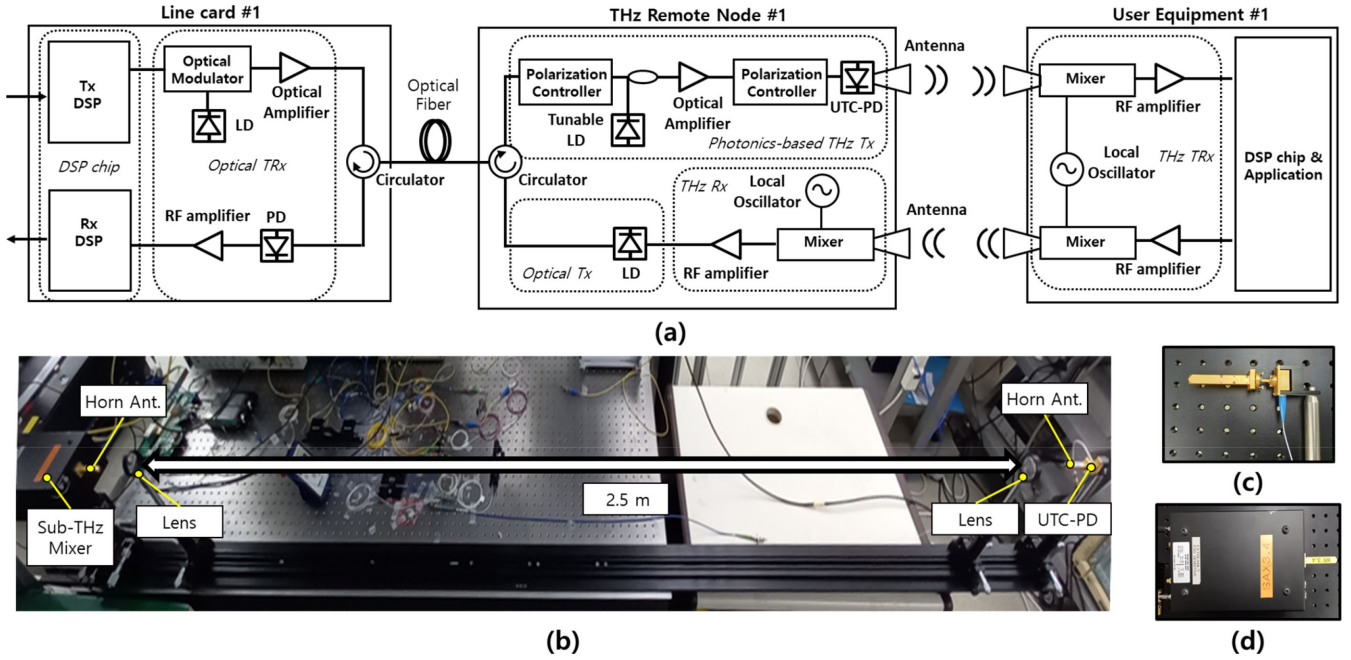Fig. 1. Schematic- diagram of our proposed THz indoor network.

Fig. 2. (a) Detailed link structure for a single data path. (b)–(d) Photographs of established link and sub-THz components. (b) 2.5 m transmission link. (c) UTC-PD. (d) sub-THz mixer.

polarization alignment. At the UTC-PD, a sub-THz-band beat signal is generated and transmitted to the wireless channel with an antenna. In the user equipment, the sub-THz-band signal is down-converted to the intermediate frequency (IF) band using an electronics-based mixer. Then, it is delivered to the DSP chip after the RF amplification procedure. The IF band signal is digitally down-converted to baseband at the DSP chip. For upstream transmission, the user equipment generates a sub-THz-band signal using an electronics-based mixer, which is then transmitted to the THz RN. At the THz RN, the upstream sub-THz-band signal is down-converted to the IF band by another electronic-based mixer. For cost-effective optical transmission, the laser is directly modulated by the converted IF band signal. The directly modulated optical signal is delivered by the optical fiber and received by the PD in the OHU. The received signal is amplified and digitally down-converted to baseband in the receiver (Rx) DSP. The photographs of the established link and sub-THz components are shown in the Fig. 2(b)–(d).

III. DOWNSTREAM TRANSMISSION WITH PHOTONICS-BASED TECHNOLOGY

A. Experimental Setup for Downstream Transmission

To investigate the system performance, we established an experimental setup using commercially available optical/electrical components. Fig. 3(a) depicts the established experimental setup for downstream transmission. In this setup, an arbitrary waveform generator (AWG, Keysight M8194A), which has a maximum sampling rate of 120 GSa/s and an analog bandwidth of 45 GHz, was used to generate a single-carrier 16-QAM baseband signal. An IQ Mach-Zehnder modulator (MZM, Fujitsu FTM 7977HQA) with a 20-GHz bandwidth was utilized as an optical modulator. An erbium-doped fiber amplifier (EDFA) was used to amplify the optical signal. A single-mode fiber (SMF) was employed to configure the fiber-optic link. The fiber launch power was set to ∼+7 dBm, which was sufficiently low to avoid the fiber nonlinear effect. The output power of the tunable laser
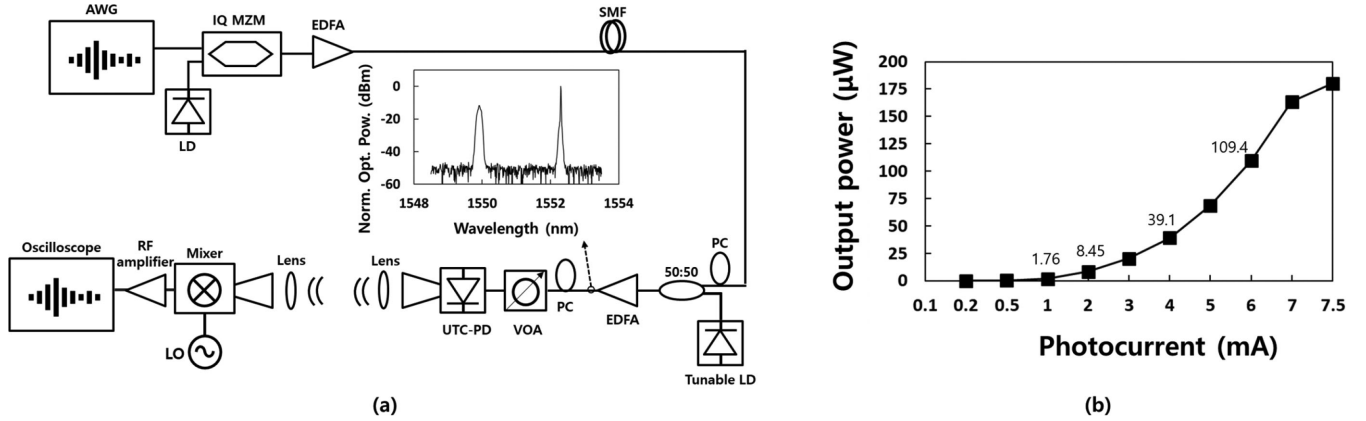
Fig. 3.   (a) Experimental setup for downstream transmission. (b) Output power of the UTC-PD as a function of photocurrent and optical input power at a carrier frequency of 300 GHz.

diode was adjusted to be the same as the transmitted optical signal power to maximize the output power of the UTC-PD (NEL J-band photomixer). The wavelength separation of the two input lights for the UTC-PD was ~2.4 nm (1549.95 nm and 1552.35 nm), with a corresponding frequency of 300 GHz. Two polarization controllers (PCs) were used for polarization alignment, and a variable optical attenuator (VOA) was utilized to adjust the input optical power to the UTC-PD. The inset shows the measured optical spectrum at the input of the UTC-PD, which is modulated with a 100 Gb/s 16-QAM signal.

To establish a wireless link, two antennas (VDI DH WR3.4) with a gain of 26 dBi and two lenses (Thorlabs TPX100) with a focal length of 10 cm were used. To receive a sub-THz-band wireless signal, an electronics-based mixer (VDI SAX3.4) was employed. The bandwidth of the mixer was 40 GHz, and the insertion loss was 14 dB. The frequency of the local oscillator was 280 GHz. The frequency mismatch between the local oscillator and the 300-GHz carrier frequency was used to generate an IF to digitally decompose the IQ signal. The received signal was captured using an 80-GSa/s real-time oscilloscope (Lecroy MCM-Zi-A) with a 36-GHz analog bandwidth. Fig. 3(b) depicts the output power of the UTC-PD at 300 GHz as a function of the photocurrent and optical input power. The output power was measured using a calorimeter-style power meter (VDI PM5). The output power values were 1.76 μW, 8.45 μW, 39.1 μW, and 109.4 μW for photocurrents of 1 mA, 2 mA, 4 mA, and 6 mA, respectively.

Fig. 4 shows the DSP structures for sub-THz-band signal transmission. In the Tx DSP, a pseudorandom binary sequence (PRBS) with a 2^{15}-1 pattern length was generated and mapped into a 16-QAM signal format. Before transmitting the signal, preambles were inserted. The purpose of the preambles was two-fold. The first was for synchronization, to find a start frame. The second was to apply the Chinese remainder theorem-based frequency offset estimation algorithm, which provides a wide range of frequency offset compensation [16]. The length of the preambles was 288 symbols. The preambles are transmitted at the start of transmission only. After adding the preambles, the signal was resampled to 100 GS/s and shaped by a
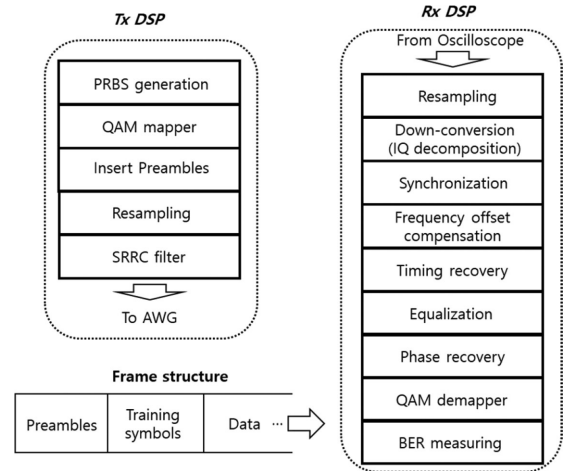

Fig. 4.   DSP structures for sub-THz-band signal transmission.

square-root-raised-cosine (SRRC) filter with a roll-off factor of 0.4. The transmitted frame structure is shown in the lower part of Fig. 4. The first 3840 symbols were used to train the adaptive filter in the receiver DSP.

At the receiver DSP, the received signal was resampled to two samples/symbols, and it was down-converted with IQ decomposition. Synchronization and frequency offset compensation were then performed using the preambles. Timing recovery based on the square-timing recovery algorithm was performed [18]. After the timing recovery, the signal was equalized with a radius-directed equalizer algorithm [19]. For carrier phase recovery, a blind-phase search algorithm was applied [20]. To estimate the carrier phase accurately with the reduced possibility of cyclic slip, the carrier phase was estimated in two steps: first, coarse estimation was performed using an averaged phase of 128 symbols; then, fine estimation was performed using an averaged phase of 20 symbols. After phase recovery, the 16-QAM symbol was demodulated, and the BERs were calculated. In our experiment, the length of the bit sequence was ~1.4×10^5 bits, excluding training bits.
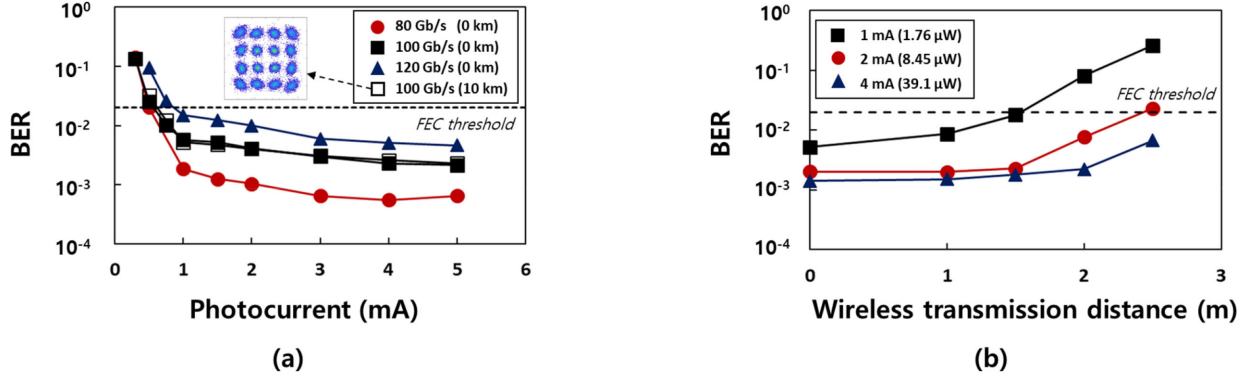
Fig. 5. Measured BERs at a carrier frequency of 300 GHz. (a) BER curves as a function of photocurrent with a short (∼3 cm) wireless distance for various data rates. Filled markers were measured with a 0-km optical fiber, and unfilled markers were measured with 10-km optical fiber. (b) BER curves as a function of wireless transmission distance with a 10-km optical fiber for various photocurrents.

B. Experimental Results for Downstream Transmission

Fig. 5(a) shows the measured BER curves as a function of photocurrent with a short wireless distance (∼3 cm). The BER curves were measured using a 0-km optical fiber (filled symbols). As shown in this figure, BER values less than the soft decision-forward error correction (SD-FEC) threshold (2.0×10^{-2}) [21] were achieved. Note that the overhead of the SD-FEC is 20% (net data rate: 80 Gb/s). Error floors were observed when the photocurrent reached 4 mA. This might be due to the phase noise. As shown in the inset of Fig 5(a), an elliptical constellation was observed. This means that the phase noise affects the transmission performance. The phase noise originated from free-running lasers and the multiplied electrical local oscillator (LO). It should be noted that the sub-THz-band signal was generated by multiplication by 12 times of the low-frequency LO signal in the sub-THz mixer. At the same time, the phase noise of the low-frequency LO was enhanced by 144 times (square of 12). To investigate the BER degradation caused by optical transmission, BERs after 10-km transmission were measured (unfilled symbols). There was no significant difference between the 10-km optical transmission and the 0-km optical transmission. This means that the chromatic dispersion induced by the 10-km optical fiber (∼170 ps/nm) was mostly compensated by the Rx DSP. Note that because the optical transmission distance in an indoor network is only a few kilometers for most practical cases, a 10-km optical fiber length might be sufficient to examine the transmission performance degradation caused by optical fibers.

Fig. 5(b) shows the transmission results over the wireless distance. For all measurements, a 10-km optical fiber was used. We successfully achieved 2.5-m wireless transmission at ∼8.46 μW THz Tx power. It is worth noting that the wireless transmission distance is restricted by the limited space. Because the sub-THz output power from the UTC-PD can be increased further, as shown in Fig. 3(b), we can expect better results when our experimental environment is improved. The maximum achievable transmission distance can be estimated as follows: Since the sub-THz link can be assumed as a free-space channel, the link loss is determined by FSPL. The FSPL can be derived from Friis

transmission formula as below,

$$FSPL = \left(\frac{4\pi d}{\lambda}\right)^2 \quad (1)$$

where λ is the wavelength, and d is the wireless transmission distance. As shown in (1), the FSPL is proportional to the square of the transmission distance. Thus, if Tx output power is increased by N times, the achievable transmission distance will be increase by $N^{1/2}$. Note that 8.46 μW Tx power was required for 2.5 m wireless transmission. Therefore, if the THz Tx power is set to 109.4 μW (photocurrent: 6 mA), the maximum achievable transmission distance is expected to be ∼9 m (2.5 m × $(109.4/8.46)^{1/2}$).

C. Scalability

As shown in Fig. 2, the line card in the OHU is one-to-one mapped with the THz RN. One approach to expand the system capacity is to increase the number of THz RNs connected with a line card. For this, $1 \times N$ optical power splitters can be used by considering an additional optical link loss of $10 \times \log(N)$ dB. To identify the accommodable number of THz RNs, it is necessary to investigate the impact of the optical link loss on the transmission performance.

It is easy to predict that the link loss affects the THz Tx power from the UTC-PD. The relationship among THz Tx power (P_{THz}), THz RN input optical power (P_{RN}), and tunable LD output power (P_{TLD}) can be simply expressed as follows:

$$P_{THz} \propto G^2 P_{RN} P_{TLD} \quad (2)$$

where G is the gain of the EDFA in the THz RN. It is reasonable to assume that the total output power from the EDFA (i.e., input power to the UTC-PD) remains constant at the designed level by using the gain-control function of the EDFA or operating the EDFA under power-saturation conditions, to operate under optimal conditions and avoid damage to the UTC-PD. Then, the input power of the UTC-PD $(P_{UTC\text{-}PD})$, which is equal to the output of the EDFA (i.e., $G(P_{RN} + P_{TLD})$), remains constant. If G is substituted using $P_{UTC\text{-}PD}$ and P_{TLD}, the relationship
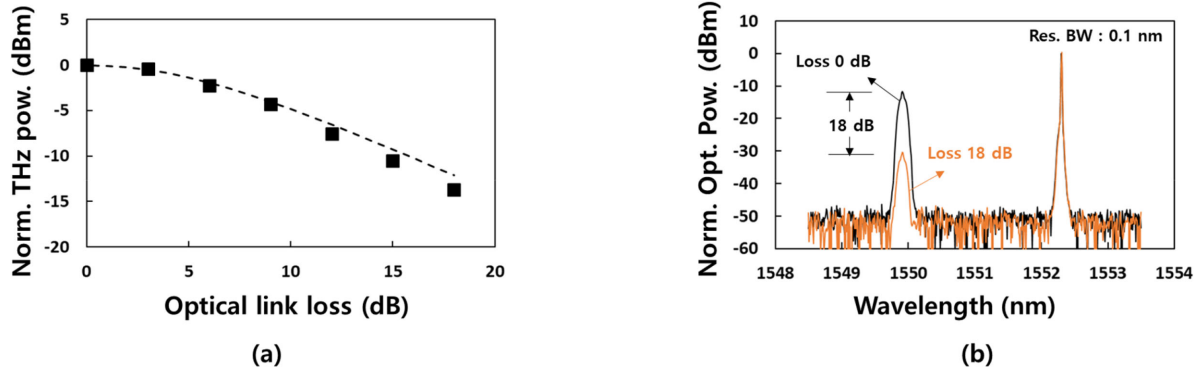
Fig. 6.   (a) Measured and calculated THz Tx power from the UTC-PD at 300 GHz as a function of optical link loss. (b) Measured optical spectra with link losses of 0 dB and 18 dB link. The spectra on the left is the transmitted signal from OHU, and the spectra on the right is the tunable laser output in the THz RN.

between P_{THz} and P_{RN} can be expressed as follows:

$$P_{THz} \propto \frac{P_{UTC-PD}{}^2 P_{TLD}}{(P_{RN} + P_{TLD})^2} P_{RN} \qquad (3)$$

For the experimental investigation, we placed a variable optical attenuator in front of the THz RN and measured the THz Tx power as a function of the optical link loss. In the measurement, the photocurrent was fixed at 4 mA (optical input power = ~12.5 dBm). At the zero-link loss, the optical powers of the two input lights were the same. The measured sub-THz power (square symbols) and calculated sub-THz power (dotted line) from (3) are shown in Fig. 6(a). As expected, they nearly match.

Another degradation can be caused by the optical signal noise ratio (OSNR) because of the decrease in the EDFA input power. The measured normalized optical spectra for link losses of 0 dB and 18 dB are shown in Fig. 6(b). The resolution bandwidth was 0.1 nm. The spectra on the left are the transmitted signals from the OHU, and the spectra on the right are the tunable laser outputs in the THz RN. The OSNR of the tunable laser output is maintained at a high level (>50 dB) because the tunable laser provides constant optical power, regardless of the link loss. However, the OSNR of the THz RN input signal decreased because of the link loss. With a link loss of 18 dB, the measured OSNR was 31.7 dB.

The BER values as a function of the optical link loss were also measured, as shown in Fig. 7. The optical and wireless transmission distances were 10 km and ~3 cm, respectively. The BERs increased with link loss. To meet the SD-FEC threshold, the allowable link losses for photocurrents of 1 mA, 2 mA, and 4 mA are 6 dB, 12 dB, and 18 dB, respectively. Note that the sub-THz output power from the UTC-PD is proportional to the square of the photocurrent; thus, the sub-THz power is increased by 6 dB by doubling the photocurrent. As shown in Fig. 7, a link loss of 6 dB was compensated for by doubling the photocurrent. This means that the dominant penalty was a result of the decrease in the sub-THz output power from the UTC-PD. According to the measured data, the maximum number of THz RNs is 64 (corresponding to a link loss of 18 dB), which can be accommodated by a single line card in the OHU. However, the number of accommodatable THz RNs should be carefully determined with the power budget of the sub-THz wireless link.
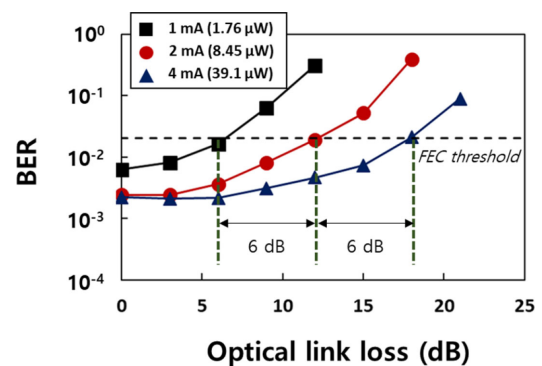

Fig. 7.   Measured BER values as a function of the optical link loss for various photocurrents. The optical and wireless transmission distances were 10 km and ~3 cm, respectively. The carrier frequency was 300 GHz.

It should be noted that the effect of link loss differs according to the location of the tunable laser. If the tunable laser is located in the OHU, the power balance is not changed by the link loss at the input port of the UTC-PD. Then, if the UTC-PD input power is kept constant by the EDFA with the gain control function, the THz Tx power from the UTC-PD will not vary with the link loss. However, this leads to an OSNR-induced penalty. In addition, the EDFA should provide additional gain corresponding to the link loss. If the EDFA fails to compensate for this link loss, the THz Tx power from the UTC-PD will be decreased by the square of the link loss, as expected from (2).

D. Tunability

In the experiment, we demonstrated 100 Gb/s transmission performance downstream. However, to meet the 6G requirement (1 Tb/s), the data rate should be increased further. One of the most promising candidates is to employ FDM in the sub-THz-band. When a photonics-based approach is used, frequency multiplexing can be easily performed in the optical domain. This is advantageous because the mature technology of wavelength division multiplexing in optical communications can be applied. For multiplexing, the THz Tx should cover a wide range of frequencies in the sub-THz-band. To confirm the operation over a wide frequency range, the tunability of the THz
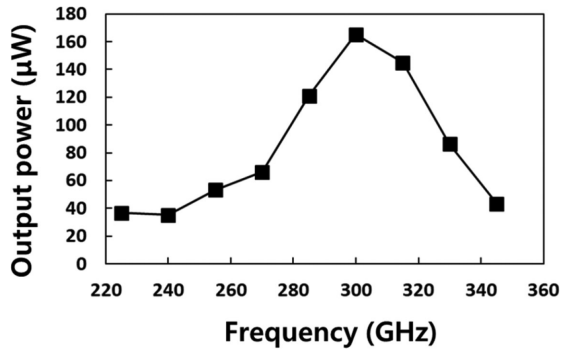
Fig. 8. Output power from the UTC-PD as a function of carrier frequency at a photocurrent of 7 mA.
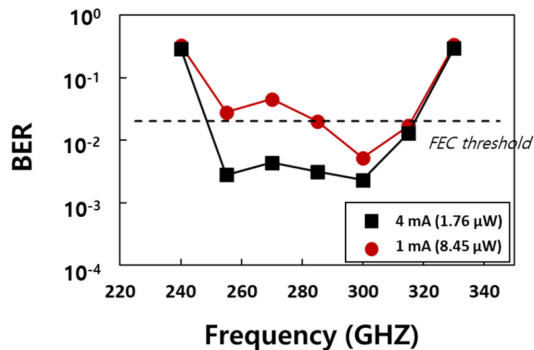

Fig. 9. Measured BERs as a function of sub-THz carrier frequency. Optical and wireless transmission distances were set to 0 km and ~3 cm, respectively.

Tx was investigated. Fig. 8 shows the measured output power of the UTC-PD with varying wavelength of the tunable laser. The photocurrent in the measurements was fixed at 7 mA. As shown in this figure, the sub-THz carrier frequency could be adjusted in the entire WR3.4 band (220–330 GHz). We did not obtain sufficient power at both ends of the WR3.4 band because the UTC-PD was designed to generate maximum power near 300 GHz [22], and the antennas were fabricated to cover the WR3.4 band. If the UTC-PD was designed to operate in a wider frequency range, the frequency flatness would be improved.

To confirm the system operation in the entire WR3.4 frequency band, we measured BERs in the WR3.4 band with a 0-km optical transmission distance and short (~3 cm) wireless distance. Fig. 9 shows the measured BERs. Except for the edges of the band, BER values less than the SD-FEC threshold were achieved when the photocurrent was set to 4 mA. The frequency-dependent BER characteristics can be identified by measurement with a photocurrent of 1 mA. The shape of the BER curve was nearly inversely proportional to the shape of the sub-THz output power from the UTC-PD, as illustrated in Fig. 8.

IV. UPSTREAM TRANSMISSION WITH ELECTRONICS-BASED TECHNOLOGY

A. Experimental Setup for Upstream Transmission

Although photonics-based technology has the advantage of high-speed transmission, its bulkiness and high energy

consumption limit practical deployment. For relatively low-speed transmission, electronics-based sub-THz-band signal generation is more attractive than the photonics-based approach. Thus, we utilized an electronics-based technology for upstream transmission. Fig. 10(a) shows the experimental setup used to investigate the performance of the uplink. The transmitted data rate was 25 Gb/s, assuming 4:1 downlink/uplink data rate ratio. With consideration of lower data rate, a QPSK signal format (instead of 16 QAM) was chosen to reduce required received sub-THz power. The 25 Gb/s single-carrier QPSK signal with an IF frequency of 9.75 GHz was generated using an AWG. The SRRC filter was digitally applied with a roll-off factor of 0.3. The QPSK signal was up-converted to the sub-THz-band using an electronics-based sub-THz mixer 1 (VDI SAX3.4). The sub-THz output power was ~0.5 μW (−33 dBm), which was the maximum achievable output power without damage. The local oscillator frequency of the mixer was set to 300 GHz. There were two duplicated sub-THz-band signals, centered at 300 ± 9.75 GHz, as depicted in Fig. 10(b). After wireless transmission with two antennas and two lenses, the sub-THz-band signal was received using sub-THz mixer 2. The sub-THz-band frequency of mixer 2 was 280.5 GHz. As a result, the center frequencies of the received signals were located at 9.75 GHz and 29.25 GHz, as shown in Fig. 10(c). For cost-effectiveness, 10 GHz-class directly modulated distributed feedback laser diode (DFB-LD) was used to generate optical signal. Thus, the signal at 29.25 GHz was filtered out by limited modulation bandwidth of the DFB-LD. The signal centered at 9.75 GHz was transmitted over the SMF. An RF amplifier and variable RF attenuator were also employed to obtain an optimal modulation index for achieving better optical transmission performance. The wavelength was 1550.53 nm, and the fiber launch power was +5 dBm. The signal was received by the photodiode after 10 km of the SMF. The EDFA and variable optical attenuator were used to adjust the received optical power. The received signal was captured by a real-time oscilloscope for the Rx DSP. The architecture of the Rx DSP was the same as that of the downlink, except for the signal format.

B. Experimental Results for Upstream Transmission

First, we examined the impact of the optical transmission. For this purpose, we measured the BER curves as a function of the received optical power for various optical fiber lengths with short (~3 cm) wireless transmission distances. Fig. 11(a) shows the results. The BERs decreased with an increase in the received optical power, and they were saturated at −2 dBm. Unlike in the downstream transmission case, BER degradation by fiber-optic transmission was observed. This was due to the frequency distortion originating from the interplay between the chirp characteristics of directly modulated DFB-LD and chromatic dispersion of optical fibers [23]. Although the measured BERs were degraded, they were still satisfied with the 20% overhead SD-FEC threshold (net data rate: 20 Gb/s). Fig. 11(b) shows the measured BER as a function of the wireless transmission distance. In the measurement, the THz Tx power was set to −33 dBm, and the received optical power was fixed at +2 dBm.
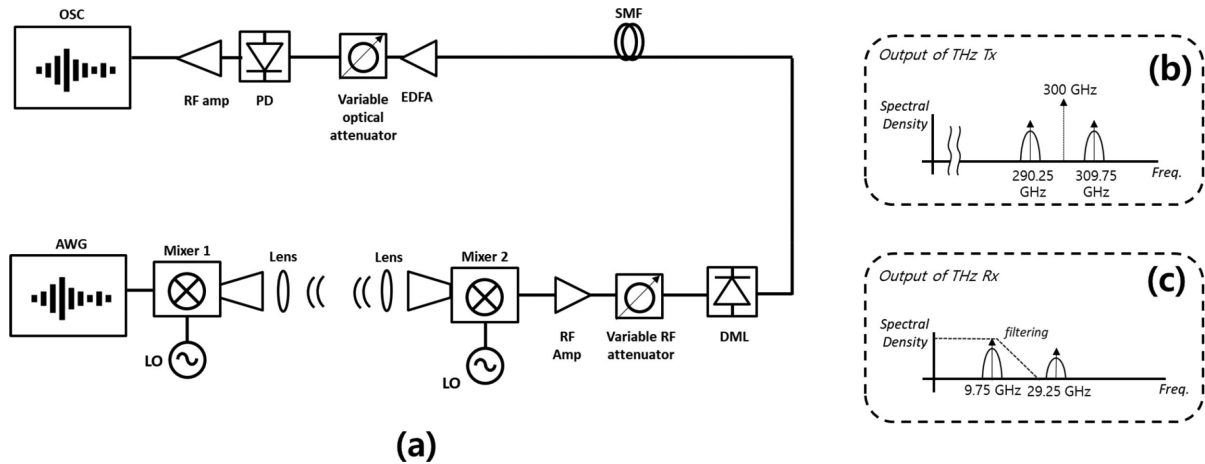
Fig. 10.   (a) Experiment setup for upstream transmission. (b) Spectrum of THz Tx output from mixer 1. (c) Spectrum of THz Rx output from mixer 2.
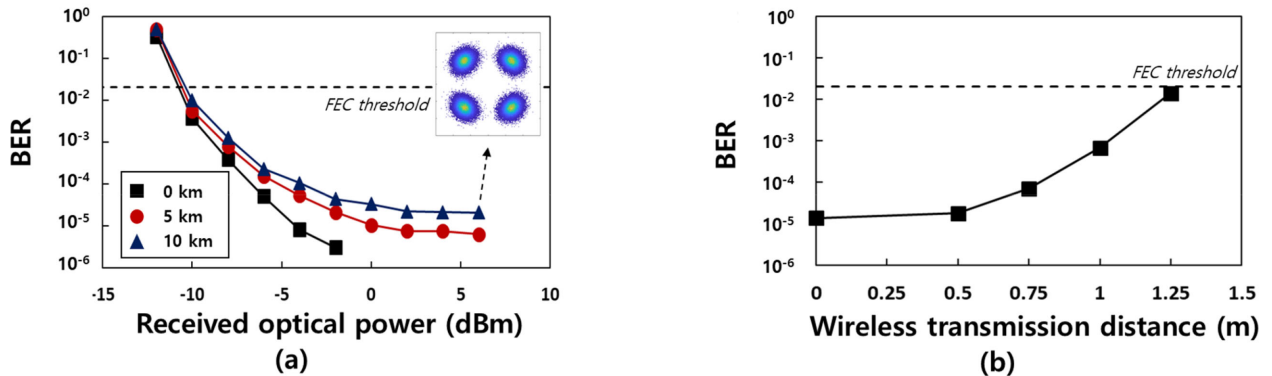

Fig. 11.   (a) Measured BER curves as a function of received optical power with various optical transmission distances. The sub-THz transmitting power was ∼0.5 μW, and the wireless distance was ∼3 cm. (b) Measured BERs as a function of wireless transmission distance. The optical transmission distance was 10 km, and the received optical power was +2 dBm.

As shown in this figure, the maximum achievable transmission distance was 1.25 m. The maximum transmission distance was mainly limited by the low THz Tx power ($\sim$0.5 μW). To improve the maximum achievable transmission distance, it is possible to adopt a sub-THz-band amplifier.

Before proceeding, we would like to discuss scalability and tunability issues for uplink. The optical link loss due to the use of a power splitter results in a power penalty in the optical transmission. As shown in Fig. 11(a), the required optical power received to meet the SD-FEC threshold was -10 dBm. If we consider a +5 dBm fiber launch power for the uplink and a 2-dB loss of the 10 km optical fiber, the estimated power margin is 13 dB. If an additional EDFA with a 20-dB gain is utilized for the uplink, the power margin can be increased to 33 dB. Thus, the power margin of the uplink is not as tight as that of the downlink. It should be emphasized that the scalability of the indoor network would be considered not by the uplink, but by downlink. With regard to tunability, there is less necessity of FDM for the upstream transmission because its required data rate is relatively lower than that of the downlink. Therefore, it is desirable to consider tunability only in the downstream direction in most cases.

V. Remaining Issues For Real-field Deployment

A. Output Power of THz Transmitter

We have thus far demonstrated the technical feasibility of our proposed THz indoor network experimentally. Despite this successful demonstration, there remain several issues to overcome. The most critical issue is the limited THz Tx power. As described in Section III, the wireless transmission distance was limited to a few meters, which is not sufficient to realize a practical wireless link. In addition, two lenses were used to compensate for the FSPL in our experiment. To eliminate them, an additional power margin of approximately 20 dB is required [8].

Several promising technologies have been developed to increase the THz Tx power. In a phonics-based approach using UTC-PD, it was reported that the output power can be increased to 1000 μW by combining the output of multiple UTC-PD chips [24]. Similarly, the THz Tx power can be increased by manufacturing an array of THz Tx chips.

A sub-THz-band amplifier will be the ultimate solution to increase the power budget limited by the FSPL. There have been several demonstrations of sub-THz-band signal transmission with sub-THz-band amplifiers that operate near 300 GHz [6],
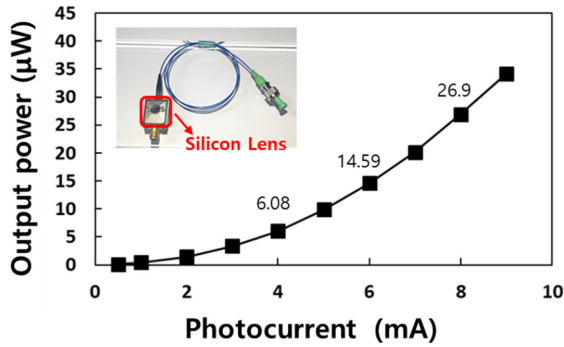
Fig. 12. Output power at 300 GHz as a function of the photocurrent of UTC-PD with a lens collimator. Inset shows an image of the UTC-PD.

Fig. 13. Measured BERs as a function of wireless transmission distance with 10-km optical transmission.

[11]. If two 20-dB amplifiers are applied at both Tx and Rx, the wireless transmission distance will be sufficiently extended. Unfortunately, the sub-THz-band amplifier has a limited operating frequency range in the sub-THz-band. This may limit the tunability of the output center frequency of the THz Tx; thus, one of the next goals will be to provide a sub-THz amplifier with a flat and wide frequency response.

B. Integration of Optical Components

The photonics-based THz Tx includes many different types of photonic elements, including optical sources, optical modulators, optical couplers, and optical attenuators. To reduce the form factor and energy consumption, photonic integration technology has been extensively developed. For example, non-return-to-zero (NRZ) signal transmission using a photonic integrated circuit at a frequency of ~300 GHz has been demonstrated [25]–[26]. We are also developing an integrated sub-THz-band signal transmitter based on silicon photonics. As an intermediate result of our efforts, we reported 40 Gb/s NRZ transmission with a silicon-based photonic integrated circuit [24]. Because silicon photonics is compatible with industrial CMOS technologies, we expect that it will enable high-volume production at a low cost per device.

C. Antenna With Small Form-Factor

The physical size of the components should be considered for commercialization of sub-THz-band communication technology. One of the largest components is the antenna. As an example, the length of the diagonal horn antenna used in our experiment was 5.6 cm, which can be a challenging issue for system and device designers.

One of the methods to reduce the antenna size is to use a silicon lens instead of a horn antenna. For several years, we have developed a UTC-PD with a lens collimator [28]. An image of the UTC-PD is shown in the inset of Fig. 12. As shown in this figure, the physical size can be significantly reduced. The measured sub-THz output power from the lens-type UTC-PD at 300 GHz is shown in Fig. 12. The measured output power values were 6.08 μW, 14.59 μW, and 26.9 μW for photocurrents of 4 mA, 6 mA, and 8 mA. Fig. 13 shows the measured BERs as a function of the wireless transmission distance. A 10-km

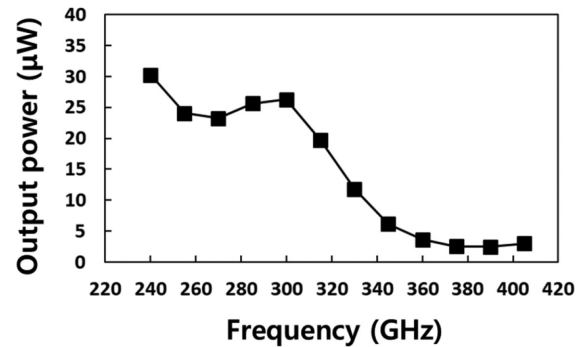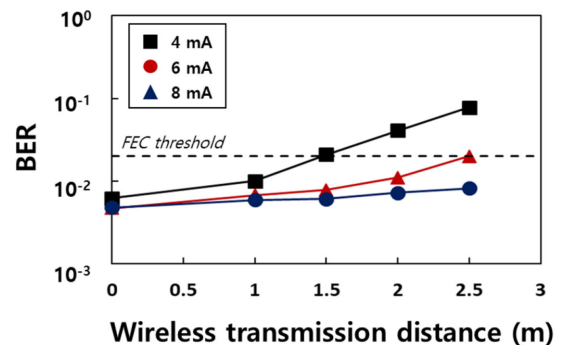Fig. 14. Measured output power from UTC-PD with a lens collimator as a function of frequency at a photocurrent of 8 mA.

optical fiber was used for optical transmission. As shown in this figure, 2.5-m wireless transmission was successfully achieved with a 16-QAM signal when the photocurrent was set to 6 mA (14.59 μW).

Another advantage of the lens collimator is broadband tunability, as the silicon lens does not limit the usable frequency range. The measured output power as a function of the carrier frequency is shown in Fig. 14. The photocurrent in this measurement was fixed at 8 mA. Because of the intrinsic characteristics of the UTC-PD, the output power tends to decrease as the carrier frequency increases. The dip near 260 GHz might be caused by interference due to the misaligned silicon-lens inside the UTC-PD module.

The measured BERs as a function of frequency are shown in Fig. 15. The measurement was performed with a 0-km optical transmission distance and short (~3 cm) wireless distance with a 100 Gb/s 16-QAM signal. Two types of mixers (VDI WR 3.4 and VDI WR 2.8) were alternately employed to extend the operating frequency range of the THz Rx. It was confirmed that the measured BERs still satisfied the SD-FEC threshold for the entire frequency range of the WR3.4 (220–330 GHz) and WR 2.8 (260–400 GHz).

D. Polarization Insensitivity

Another challenging issue for photonics-based THz Tx is polarization alignment. To generate a beat signal in the UTC-PD, the polarization of the two input lights and the UTC-PD itself
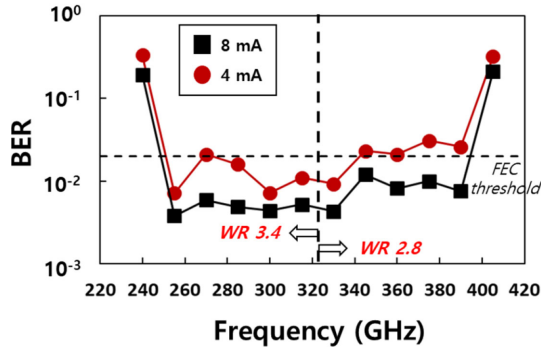
Fig. 15. Measured BERs as a function of sub-THz carrier frequency employing the UTC-PD with a lens collimator. The optical and wireless transmission distances are 0 km and ∼3 cm, respectively.

should be carefully aligned. In most demonstrations, including the experiment in this study, the polarization is aligned manually. However, this is not practical because the polarization is randomly rotated by time and temperature in most practical cases. Polarization-maintaining components may be helpful, but the optical fiber still rotates the polarization. The polarization control can be automated using a polarization-variable wave plate while monitoring the state of the polarization. However, this solution may not be affordable in many cases.

The simplest method is to use polarization multiplexing and 2×2 multi-input multi-output (MIMO) transmission techniques [5], [7], [29]. In these methods, two independent user-data are transmitted for each polarization. After optical transmission, the two polarizations are separated by a polarization beam splitter. Then, each polarized light is transmitted by two independent wireless links. The rotated polarization can be restored using 2×2 MIMO processing. These methods are promising because they not only solve the polarization issue, but also double the data rate, although it requires additional wireless links.

Another approach to ease the polarization alignment issue is to use a polarization-insensitive UTC-PD. The photodiode is not inherently polarization-sensitive, so the polarization dependence of the UTC-PD originates from the internal structure that collects the optical beam. With careful modification of the internal structure, polarization-insensitive UTC-PDs have been demonstrated [30]. By applying this, we believe that the polarization controller in front of the UTC-PD can be removed.

E. Automatic Beam Steering

Because of the high directivity of the sub-THz wave, automatic beam steering is necessary to minimize power loss. Fast beam steering provides an additional advantage for the capability to support multiple devices by rapid path switching.

Several promising methods have been proposed for this purpose. For example, a sub-THz beam can be steered by adjusting the relative position between the antenna and the lens [31]. Another approach for beam steering is to adopt an integrated phased array [32]. In addition, advanced beam steering technologies have been developed, such as leaky wave antennas [33] and reflector arrays [34]. However, advances in automatic beam

steering in sub-THz-band wave are still limited, so much work remains to be done.

VI. Summary

In this paper, we proposed an indoor network with sub-THz-band communication technology for 6G applications. The system was composed of three types of components: an OHU, THz RN, and user equipment. The OHU and THz RN were connected by a fiber-optic link, and the THz RN and user equipment were connected by a wireless link. The THz RN provided an interface between the two different types of links. For downstream transmission, which is required to support high-speed transmission, a photonics-based approach for sub-THz-band signal generation was used to take advantage of optical components with ultra-wide bandwidth and low-loss characteristics. Because upstream transmission has a relatively lower throughput requirement, an electronics-based approach was applied for cost-effectiveness and low energy consumption.

To investigate the system performance, we established an experimental setup using commercially available components. To recover the signal after transmission, a DSP was designed, focusing on compensation for a wide-range frequency offset. Additionally, a two-step carrier-phase estimation was applied to reduce the probability of cyclic slip. Throughout our experiment, we successfully achieved 100 Gb/s 16 QAM downstream transmission and 25 Gb/s QPSK upstream transmission. In both cases, the optical transmission distance was 10 km, which is considered sufficient for indoor network applications. We also achieved a wireless transmission distance of 2.5 m (potentially 9 m) and 1 m for downstream and upstream, respectively. To expand the system capacity, an optical power splitter can be used. To investigate scalability, the effect of the optical link loss induced by the power splitter was examined. FDM is a promising technology for increasing the data rate. To support the FDM, the THz Tx should operate over a wide frequency range in the sub-THz-band. We experimentally confirmed the operation of the photonics-based THz Tx in the WR 3.4 band.

Finally, we discussed the remaining issues in realizing a practical system. The addressed issues were the limited THz Tx power, bulkiness of the optical components, large-sized antenna, polarization dependency, and automatic beam steering. Among them, we introduced some promising potential solutions, including our efforts, such as silicon-based integration and a UTC-PD with a lensed collimator. We hope that our proposed sub-THz-band indoor network will be realized in the upcoming 6G era.

References

[1] W. Saad, M. Bennis, and M. Chen, "A vision of 6G wireless systems: Applications, trends, technologies, and open research problems," *IEEE Netw.*, vol. 34, no. 3, pp. 134–142, May/Jun. 2020.

[2] Y. Zhou *et al.*, "Service-aware 6G: An intelligent and open network based on the convergence of communication, computing and caching," *Digit. Commun. Netw.*, vol. 6, no. 3, pp. 253–260, 2020.

[3] S. Chen, Y.-C. Liang, S. Sun, S. Kang, W. Cheng, and M. Peng, "Vision, requirements, and technology trend of 6G: How to tackle the challenges of system coverage, capacity, user data-rate and movement speed," *IEEE Wireless Commun.*, vol. 27, no. 2, pp. 218–228, Apr. 2020.

[4] S. Dang, O. Amin, B. Shihada, and M.-S. Alouini, "What should 6G be?," *Nature Electron.*, vol. 3, pp. 20–29, 2020.

[5] P. Rodriguez-Vazquez, J. Grzyb, B. Heinemann, and U. R. Pfeiffer, "A QPSK 110-Gb/s polarization-diversity MIMO wireless link with a 220–255 GHz tunable LO in a SiGe HBT technology," *IEEE T Microw. Theory*, vol. 68, no. 9, pp. 3834–3851, Sep. 2020.

[6] H. Hamada *et al.*, "300-GHz-band 120-Gb/s wireless front-end based on InP-HEMT PAs and mixers," *IEEE J. Solid-State Circuits*, vol. 55, no. 9, pp. 2316–2335, Sep. 2020.

[7] C. Castro, R. Elschner, T. Merkle, C. Schubert, and R. Freund, "100 Gb/s real-time transmission over a THz wireless fiber extender using a digital-coherent optical modem," in *Proc. Opt. Fiber Commun. Conf. (OFC) 2020*, 2020, Paper M4I.2.

[8] K. Liu *et al.*, "100 Gbit/s THz photonic wireless transmission in the 350-GHz band with extended reach," *IEEE Photon. Technol. Lett.*, vol. 30, no. 11, pp. 1064–1067, Jun. 2018.

[9] S. Jia *et al.*, "2 × 300 Gbit/s line rate PS-64QAM-OFDM THz photonic-wireless transmission," *J. Lightw. Technol.*, vol. 38, no. 17, pp. 4715–4721, Sep. 2020.

[10] S.-R. Moon, M. Sung, J. K. Lee, and S.-H. Cho, "Cost-effective photonics-based THz wireless transmission using PAM-N signals in the 0.3 THz band," *J. Lightw. Technol.*, vol. 39, no. 2, pp. 357–362, Jan. 2021.

[11] T. Harter *et al.*, "110-m THz wireless transmission at 100 Gbit/s using a kramers-kronig schottky barrier diode receiver," in *Proc. Eur. Conf. Opt. Commun. (ECOC 2018)*, 2018, pp. 1–3.

[12] V. Petrov, J. Kokkoniemi, D. Moltchanov, J. Lehtomäki, Y. Koucheryavy, and M. Juntti, "Last meter indoor terahertz wireless access: Performance insights and implementation roadmap," *IEEE Commun. Mag.,* vol. 56, no. 6, pp. 158–165, Jun. 2018.

[13] D. Wake, A. Nkansah, and N. J. Gomes, "Radio over fiber link design for next generation wireless systems," *J. Lightw. Technol.,* vol. 28, no. 16, pp. 2456–2464, Nov. 2010.

[14] K. Miyamoto *et al.*, "Transmission performance investigation of RF signal in RoF-DAS over WDM-PON with bandpass-sampling and optical TDM," *J. Lightw. Technol.,* vol. 31, no. 22, pp. 3477–3488, Nov. 2013.

[15] M. Sung *et al.*, "RoF-based radio access network for 5G mobile communication systems in 28 GHz millimeter-wave," *J. Lightw. Technol.,* vol. 38, no. 2, pp. 409–420, Jan. 2020.

[16] H. Y. Rha, B. G. Jeon, and H. Choi, "Simple wide range carrier frequency offset estimator for coherent optical OFDM," *IEEE Photon. Technol. Lett.*, vol. 24, no. 22, pp. 2064–2066, Nov. 2012.

[17] S.-R. Moon, E.-S. Kim, M. Sung, J. Kim, J. K. Lee, and S.-H. Cho, "Experimental investigations on upstream transmission performances in future-proof THz-band indoor network based on photonics," *Opt. Fiber Technol.*, vol. 65, 2021, Art no. 102622.

[18] M. Oerder and H. Meyr, "Digital filter and square timing recovery," *IEEE Trans. Commun.*, vol. 36, no. 5, pp. 605–612, May 1988.

[19] M. J. Ready and R. P. Gooch, "Blind equalization based on radius directed adaptation," in *Proc. Int. Conf. Acoust., Speech, Signal Process.*, 1990, vol. 3, pp. 1699–1702.

[20] T. Pfau, S. Hoffmann, and R. Noé, "Hardware-efficient coherent digital receiver concept with feedforward carrier recovery for *M*-QAM constellations," *J. Lightw. Technol.*, vol. 27, pp. 989–999, Apr. 2009.

[21] L. Zhou and D. Liu, "Symmetric 50G PON using NRZ," *IEEE 802.3 Plenary*, Mar. 2018. [Online]. Available: http://www.ieee802.org/3/ca/public/meeting_archive/2018/03/zhou_3ca_1_0318.pdf.

[22] A. Wakatsuki, T. Furuta, Y. Muramoto, T. Yoshimatsu, and H. Ito, "High-power and broadband sub-terahertz wave generation using a J-band photomixer module with rectangular-waveguide output port," in *Proc. 33rd Int. Conf. Infrared, Millimeter Terahertz Waves*, 2008, pp. 1–2.

[23] E. Bergmann, C. Kuo, and S. Huang, "Dispersion-induced composite second-order distortion at 1.5 μm," *IEEE Photon. Technol. Lett.*, vol. 3, no. 1, pp. 59–61, Jan. 1991.

[24] H.-J. Song, K. Ajito, Y. Muramoto, A. Wakatsuki, T. Nagatsuma, and N. Kukutsu, "Uni-travelling-carrier photodiode module generating 300 GHz power greater than 1mW," *IEEE Microw. Wireless Co.*, vol. 22, no. 7, pp. 363–365, Jul. 2012.

[25] G. Carpintero, S. Hisatake, D. Felipe, R. Guzman, T. Nagatsuma, and N. Keil, "Wireless data transmission at terahertz carrier waves generated from a hybrid InP-polymer dual tunable DBR laser photonic integrated circuit," *Sci. Rep.*, vol. 8, no. 1, 2018, Art. no. 3018.

[26] E. Lacombe *et al.*, "10-Gb/s Indoor THz communications using industrial Si photonics technology," *IEEE Microw. Wireless Co. Lett.*, vol. 28, no. 4, pp. 362–364, Apr. 2018.

[27] S.-R. Moon *et al.*, "Demonstration of photonics-aided terahertz wireless transmission system with using silicon photonics circuit," *Opt. Exp.*, vol. 28, no. 16, pp. 23397–23408, 2020.

[28] E. S. Lee *et al.*, "Semiconductor-based terahertz photonics for industrial applications," *J. Lightw. Technol.*, vol. 36, no. 2, pp. 274–283, Jan. 2018.

[29] X. Li, J. Yu, K. Wang, W. Zhou, and J. Zhang, "Photonics-aided 2 × 2 MIMO wireless terahertz-wave signal transmission system with optical polarization multiplexing," *Opt. Exp.*, vol. 25, no. 26, pp. 33236–33242, 2017.

[30] Y. Muramoto, H. Fukano, and T. Furuta, "A polarization-independent refracting-facet uni-traveling-carrier photodiode with high efficiency and large bandwidth," *J. Lightw. Technol.*, vol. 24, no. 10, pp. 3830–3834, Oct. 2006.

[31] P. Lu, V. Rymanov, S. Dülme, B. Sievert, A. Rennings, and A. Stöhr, "THz beam forming and beam switching using lens-assisted quasi-optical THz transmitter," in *Proc. 2017 Int. Topical Meeting Microw. Photon. (MWP)*, 2017, pp. 1–4.

[32] P. Offermans *et al.*, "Towards THz beam steering with integrated phased photomixer arrays" in *Proc. SPIE 11685, Terahertz, RF, Millimeter, Submillimeter-Wave Technol. Appl. XIV*, Mar. 2021, Art. no. 116851F.

[33] X. Fu, F. Yang, C. Liu, X. Wu, and T. J. Cui, "Terahertz beam steering technologies: From phased arrays to field-programmable metasurfaces," *Adv. Opt. Mater.*, vol. 8, no. 3, Feb. 2020, Art. no. 1900628.

[34] K. Narayanasamy, G. N. A. Mohammed, K. Savarimuthu, R. Sivasamy, and M. Kanagasabai, "A comprehensive analysis on the state-of-the-art developments in reflectarray, transmitarray, and transmit-reflectarray antennas," *Int. J. RF Microw. C. E.*, vol. 30, no. 9, pp. 1–22, Sep. 2020.

Sang-Rok Moon (Member, IEEE) received the B.S. degree in physics from the Korea Advanced Institute of Science and Technology, Daejeon, Korea, in 2008. He received the M.S. and Ph.D. degrees in electrical engineering from the Korea Advanced Institute of Science and Technology, Daejeon, Korea, in 2010 and 2015, respectively. Since 2015, he has been with the Electronics and Telecommunication Research Institute (ETRI), Daejeon, where he is currently a Senior Researcher. His current research interests include high-speed optical transmission systems, digital signal processing in optical networks, and photonics-based THz-band communication systems.

Eon-Sang Kim received the B.S. degree in electronic and information engineering from the Seoul National University of Science and Technology, Seoul, South Korea, in 2010 and the Ph.D. degree in information and communication engineering from the University of Science and Technology, Daejeon, South Korea, in 2019. Since 2019, he has been with Electronics and Telecommunication Research Institute (ETRI), Daejeon, South Korea, as a Researcher. His current research interests include next-generation optical access network, mobile fronthaul, indoor distributed antenna system, and radio-over-fiber.

Minkyu Sung received the B.S. degree in computer and communication engineering from Korea University, Seoul, Korea, in 2010 and the Ph.D. degree in computer and radio communication engineering from Korea University, in 2015. Since 2015, he has been with Electronics and Telecommunication Research Institute (ETRI), Daejeon, where he is currently a Senior Researcher. His current research interests include optical OFDM, digital signal processing, mobile fronthaul, indoor distributed antenna system, and radio-over-fiber.

Hae Young Rha received the B.S. degrees in physics from Korea University, Seoul, Korea, in 1994 and the M.S. degrees in physics from Seoul national university, Seoul, Korea, in 1996 and the Ph.D. degree in the Electronic Engineering Department, Korea Advanced Institute of Science and Technology (KAIST), Daejeon, Korea, in 2015. From 1996 to 2009, she was a Semiconductor Logic Designer with Hynix, Samsung electronics and Electronics and Telecommunication Research Institute (ETRI). Since 2015, she has been a Principal Engineer with Miro&I Co. Her research interests include the design and implementation of high-speed optical communication DSP.

Eui Su Lee received the Ph.D. degree in electronics and electrical engineering from the Korea Maritime University, Busan, South Korea, in 2013. He joined the THz Photonics Creative Research center of the Electronics and Telecommunications Research Institute (ETRI), Daejeon, South Korea, in 2013. His interests include THz time-domain spectroscopy, the application of THz parallel-plate metal waveguides, and the fabrication of photodiodes for THz generation, and Schottky barrier diodes for THz detection.

Il-Min Lee received the B.S. and M.S. degrees in electrical engineering and computer science from Seoul National University, Seoul, South Korea. From 2000 to 2003, he was an Engineer with the Optoelectronics Division of Samsung Electronics, Suwon, South Korea. In 2009, he received the Ph.D. degree in electrical engineering and computer science from Seoul National University. From 2009 to 2013, he was a Postdoctoral Researcher and a BK21 Contract Professor of Seoul National University. Since July 2013, he has been working with the Terahertz Basic Research Section of ETRI as a Senior Researcher. His current research interests include terahertz communications, imaging, spectroscopy, and terahertz nano-photonics.

Kyung Hyun Park is the Director of the Terahertz Photonics Creative Research Center, ETRI. In 1996, he received the Ph.D. degree in physics from Yonsei University, Seoul, Korea. From 1996 to 1997, he worked on large-scale photonic integrated circuits with the Microelectronic Science Laboratory, Columbia University, as a Postdoctoral Research Fellow. From 1990 to 1999, he was with the Korea Institute of Science and Technology, Seoul, South Korea, as a member of the research staff, where he was engaged in research on functional photonic devices. Since 1999, he has been with ETRI, continuing his research on photonic devices, and has been in charge of the WDM Photonic Devices Team, and the Next-Generation Photonic Device Team. He has demonstrated various photonic devices for optical communications. His current research interest focuses on the realization of THz technology using photonic devices. Dr. Park is a fellow member of SPIE and a Senior Member of OSA.

Joon Ki Lee received the M.S. degree in applied physics from the Gwangju Institute of Science and Technology (GIST), Gwangju, South Korea, in 1997 and the Ph.D. degree in electronics engineering from Chungnam National University, Daejeon, South Korea, in 2016. From 1997 to 2001, he was an Engineer with Hanwha Information and Telecommunications Corporation. Since 2001, he has been with Electronics and Telecommunications Research Institute (ETRI) in Korea, where he is currently the Managing Director of the Optical Networking Research Section. His research interests include high-speed optical transmission systems, optical transceivers, data center network, and optical-mobile converged access network.

Seung-Hyun Cho received the B.S. and M.S. degrees in electronic materials engineering from Kwangwoon University, Seoul, Korea, in 1997 and 1999, respectively. He received the Ph.D. degree in materials science and engineering from Hanyang University, Seoul, Korea, in 2010. From 1999 to 2000, he was with the Access Network Laboratory of Korea Telecom, Daejeon, South Korea. Since 2000, he has been with the Electronics and Telecommunication Research Institute, Daejeon, where he is currently Project Leader for THz short-distance transmission technology based on photonics. His current research interests include next-generation optical access network, mobile fronthaul and DAS for 5G networks, and THz wireless delivery system. He is also the Chair of IEC TC103 (transmitting equipment for radiocommunication) and a Co-Editor of G.9803 (radio over fiber systems) in ITU-T SG15/Q2.